

# Leveraging MLLM Embeddings and Attribute Smoothing for Compositional Zero-Shot Learning

Xudong Yan<sup>1</sup>, Songhe Feng<sup>1\*</sup>, Yang Zhang<sup>1</sup>, Jian Yang<sup>2</sup>, Yueguan Lin<sup>2</sup>, Haojun Fei<sup>2</sup>

<sup>1</sup>School of Computer Science and Technology, Beijing Jiaotong University <sup>2</sup>Qifu Technology

{xud\_yan, shfeng, chefzhang}@bjtu.edu.cn, {feihaojun, yangjian1, linyueguan}-jk@360shuke.com

## Abstract

*Compositional zero-shot learning (CZSL) aims to recognize novel compositions of attributes and objects learned from seen compositions. Previous works disentangle attribute and object by extracting shared and exclusive parts between image pairs sharing the same attribute (object), as well as aligning them with pretrained word embeddings to improve unseen attribute-object recognition. Despite the significant achievements of existing efforts, they are hampered by three limitations: (1) the efficacy of disentanglement is compromised due to the influence of the background and the intricate entanglement of attribute with object in the same parts. (2) existing word embeddings fail to capture complex multimodal semantic information. (3) overconfidence exhibited by existing models in seen compositions hinders their generalization to novel compositions. Being aware of these, we propose a novel framework named Multimodal Large Language Model (MLLM) embeddings and atTribute smoothIng guiDEd diseNTanglement (**TRIDENT**) for CZSL. First, we leverage feature adaptive aggregation modules to mitigate the impact of background, and utilize learnable condition masks to capture multigranularity features for disentanglement. Then, the last hidden states of MLLM are employed as word embeddings for their superior representation capabilities. Moreover, we propose attribute smoothing with auxiliary attributes generated by Large Language Model (LLM) for seen compositions, addressing the issue of overconfidence by encouraging the model to learn more attributes in one given composition. Extensive experiments demonstrate that **TRIDENT** achieves state-of-the-art performance on three benchmarks.*

## 1. Introduction

As for the study of compositional generalization ability inherent to humans, compositional zero-shot learning (CZSL)

[22, 26, 33] is proposed to enable machines to recognize unseen attribute-object compositions by leveraging knowledge of attributes and objects (*i.e.*, primitives) learned from seen compositions. Specifically, in the training phase, models are provided with images and compositional labels (*e.g.*, ripe orange and peeled apple). During the testing phase, given an image depicting a novel composition (*e.g.*, peeled orange), models are assigned to classify the image into the corresponding category [44].

Prior works [22, 27] focus on mapping the visual features and the word embeddings of compositions into a joint space. These methods have poor generalization capability to unseen compositions, as they fail to learn primitives. Therefore, recent studies [8, 14, 38] consider visual disentanglement. Among them, some prominent works deploy a triplet of images to disentangle: a given image (noted as the main image), and two supplementary images, each sharing either the same attribute or the same object as the main image. The triplet of images is treated as two image pairs for subsequent analysis. These approaches aim to disentangle attribute and object by analyzing the shared and exclusive features of the image pair, as well as aligning them with word embeddings (*e.g.*, GloVe [32]), as shown in Figure 1. Although these pioneer research studies have achieved great progress, they exhibit three limitations:

**L1:** Disentanglement is impeded due to the influence of the background and the intricate entanglement of attribute with object in the same parts of image. On the one hand, models tend to extract the background feature unique to one image in the pair as the disentangled exclusive features. On the other hand, some existing methods [36, 38] compute the similarity of image pairs for disentanglement at the spatial level. However, disentangling attribute and object at the spatial level presents significant challenges because they entangle in the same spatial features. Taking an image of ripe apple as an example, the spatial regions corresponding to the attribute "ripe" and the object "apple" are fully co-located.

**L2:** Existing word embeddings lack the depth needed to capture complex multimodal semantic information. To

\*Corresponding author

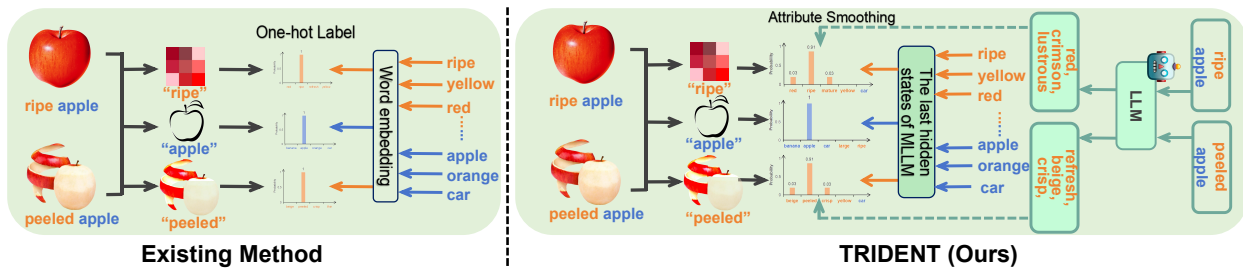


Figure 1. A general comparison between the existing method and our proposed **TRIDENT**. Note that, we only present the representation learning of an image pair sharing the object for brevity.

begin with, word embeddings, such as Word2Vec [21] and GloVe [32], are grounded in word frequency and contextual co-occurrence, rather than capturing high-level semantic nuances[39]. Moreover, the process of aligning visual features with word embeddings can be viewed as a form of cross-modal matching; however, these word embeddings are trained only in a single text modal, failing to capture cross-modal information between images and texts.

**L3:** Existing methods display excessive confidence in seen compositions, impairing their ability to generalize toward novel compositions. Due to the one-hot label used during training, these approaches are limited by learning only one attribute and object, neglecting the fact that objects naturally exhibit multiple attributes [43]. Consequently, models exhibit overconfidence in the disentangled ground-truth attribute, treating other attributes that can describe the object as negative attributes, which results in the diminished performance on unseen compositions.

To address the aforementioned limitations, we propose a novel framework named Multimodal Large Language Model (MLLM) embeddings and **atTribute smoothIng guided disE NTanglement (TRIDENT)**, which consists of three major modules: visual feature extraction, attribute-object disentanglement, and feature alignment. The first module leverages feature adaptive aggregation (FAA) modules to mitigate the impact of background noise, and exploits learnable condition masks to learn multi-granularity features to improve subsequent disentanglement. The second module aims at leveraging shared and exclusive weights of image pairs to disentangle attribute and object under the paradigm that apart from the shared features of the image pair, each image has its own exclusive features. The third module is intended to align the visual features of compositions and disentangled primitives with the last hidden states of an MLLM, LLaVA v1.5 [16], *i.e.*, MLLM embeddings. This is inspired by some works [12, 23, 24, 41], which find that the last hidden states of (M)LLM exhibit powerful representational capabilities in embedding tasks, such as retrieval and classification. Moreover, to tackle the issue that the ineffective overconfidence of the models regarding ground-truth attribute hinders them from generalizing to unseen compositions, we exploit a Large Language Model (LLM), GPT-3.5 [29] to generate auxiliary attributes

based on attribute-object compositions and perform label smoothing for attributes, *i.e.*, attribute smoothing.

In summary, the contributions of our work are three-fold:

1. We propose novel feature adaptive aggregation modules to reduce the impact of background, and utilize learnable condition masks to capture multi-granularity features for disentanglement in CZSL.
2. We employ both LLM and MLLM to guide attribute-object disentanglement by generating auxiliary attributes and representing word embeddings, respectively. To the best of our knowledge, we are the first to leverage both LLM and MLLM to advance disentanglement in CZSL task.
3. We conduct extensive experiments to evaluate our method on three CZSL benchmarks, showing that **TRIDENT** has achieved state-of-the-art performance. The source code will be released soon <sup>1</sup>.

## 2. Related Work

**Compositional zero-shot learning (CZSL).** Prior works in CZSL can be broadly divided into two main streams. One main stream is to learn representations of compositions in a joint space. SymNet [15] proposes to learn symmetry property in compositions. Co-CGE [20] leverages a Graph Convolutional Neural Network to learn compositional representations. The other main stream aims at disentangling visual representations of primitives to reduce composition learning into primitive learning. SCEN [13] leverages contrastive loss to excavate discriminative prototypes of primitives. OADis [38] disentangles primitives by affinity modules. CANet [42] learns conditional attribute conditioned on the recognized object and the input image.

More recent works [9, 18, 28] focus on leveraging the encyclopedic knowledge of pretrained vision-language models (VLM), such as Contrastive Language-Image Pre-training (CLIP) [35] and Context Optimization (CoOp) [46], to encode and align images and texts.

**Large language model (LLM).** LLMs have realized significant advancements thanks to the scaling up of training data and the increase in the number of parameters. Early models, such as BERT [6] and GPT-2 [34], initially exhibit strong capabilities in understanding and generating human-

<sup>1</sup><https://github.com/xud-yan/Trident>

like language. Subsequently, GPT-3 [4] and LLaMA [40] demonstrate great breakthroughs across numerous language benchmarks. Moreover, by performing instruction fine-tuning on LLM, ChatGPT [30] and Vicuna [5, 45] are able to comprehend and follow human instructions better.

Expanding on LLM, Multimodal Large Language Model (MLLM) incorporates a pretrained visual encoder for vision-language tasks. Flamingo [1] first integrates Vision Transformer (ViT) [7] and LLM by gated cross-attention. Recently, LLaVA [17] and LLaVA v1.5 [16] introduce visual instruction tuning to enhance instruction following capability. The visual understanding part of LLaVA v1.5 consists of a ViT and a multilayer perceptron (MLP) cross-modal connector (CMC). CMC processes visual features before the last layer of ViT, aligning the visual space of ViT with the linguistic space of LLM. We choose LLaVA v1.5 as our foundational MLLM as it has demonstrated state-of-the-art performance across various tasks.

Recently, exploring the powerful language capabilities of (M)LLM to handle representation tasks (*e.g.*, retrieval) has emerged as a prominent research domain. SGPT [23] exploits the last hidden states of LLM for the input token sequence or a special learnable token to derive representational embeddings. Subsequently, GritLM [24] applies mean pooling over the last hidden states of LLM to yield the textual embeddings. FROMAGE [12] uses a learnable token to represent the text fed into MLLM for image retrieval.

### 3. Approach

#### 3.1. Task Formulation

Compositional zero-shot learning (CZSL) aims at learning a model that can recognize unseen compositions of attributes and objects that are learned from seen compositions. Given an attribute set  $\mathcal{A}$  and an object set  $\mathcal{O}$ , the attributes and objects are composed to form a composition set  $\mathcal{C} = \mathcal{A} \times \mathcal{O}$ . The composition set  $\mathcal{C}$  is divided into two disjoint sets: the seen composition set  $\mathcal{C}_s$  and the unseen composition set  $\mathcal{C}_u$ , where  $\mathcal{C}_s \cap \mathcal{C}_u = \emptyset$  and  $\mathcal{C}_s \cup \mathcal{C}_u = \mathcal{C}$ . The model is trained with a seen training set  $\mathcal{D}_{tr} = \{(x_s, c_s)\}$ , where  $x_s \in \mathcal{X}_s$  is an image from the seen image set  $\mathcal{X}_s$  corresponding to the seen composition set  $\mathcal{C}_s$ , and  $c_s \in \mathcal{C}_s$  is the label of  $x_s$ . Following the Generalized CZSL [33], the model is evaluated on a predefined test set  $\mathcal{D}_{te} = \{(x_{te}, c_{te})\}$ , where  $x_{te} \in \mathcal{X}_{te}$  is an image from the unseen image set  $\mathcal{X}_{te}$  corresponding to the composition subset  $\mathcal{C}_{te}$  of  $\mathcal{C}$ , *i.e.*,  $\mathcal{C}_{te} \subseteq \mathcal{C}$ , and  $c_{te} \in \mathcal{C}_{te}$  is the label of  $x_{te}$ . The aim of CZSL task is to learn a model  $M : \mathcal{X}_{te} \rightarrow \mathcal{C}_{te}$  that predicts labels  $c_{te}$  from  $\mathcal{C}_{te}$  for the input images  $x_{te} \in \mathcal{X}_{te}$ .

#### 3.2. TRIDENT

As the major novelty, we propose a novel framework named MLLM embeddings and attribute smoothing guided disen-

tanglement framework (**TRIDENT**) for CZSL, as shown in Figure 2. It consists of three major modules: (1) visual feature extraction, (2) attribute-object disentanglement, and (3) feature alignment. We now detail each module of **TRIDENT** in this section.

##### 3.2.1. Visual Feature Extraction

As shown in Figure 2, we denote a given image with the attribute-object composition label (*e.g.* ripe apple) as the main image  $x^m$ , and randomly sample an image with the same attribute  $x^a$  (*i.e.*, ripe orange), as well as an image sharing the same object  $x^o$  (*i.e.*, peeled apple) to comprise a triplet image set. For the convenience of expression, we simply use  $x^{img}$  (where  $img \in \{m, a, o\}$ ) to collectively denote the images as they are processed using the same module.

**Visual feature extraction backbone.** As mentioned before, since LLaVA v1.5 is used as our fundamental MLLM, we directly leverage the visual encoder, ViT, and cross-modal connector (CMC) from the model to extract visual features. Specifically, the image  $x^{img}$  is partitioned into  $n$  patch tokens, which are subsequently put into ViT along with the [CLS] token. Afterward, the output of patch tokens before the last layer of ViT is fed into the CMC module, as implemented in LLaVA v1.5. To align the dimension of patch tokens output by CMC with that of [CLS] token produced by ViT, the patch tokens output by CMC are input into a linear layer. Consequently, we obtain one feature vector of [CLS] token  $J_{cls}^{img} \in \mathbb{R}^d$  and a patch feature matrix of  $n$  patch tokens  $F_{patch}^{img} \in \mathbb{R}^{n \times d}$ , where  $d$  is the dimension of the features.

**Local features extraction.** Intuitively, the composition (*e.g.*, ripe apple) only occupies a few parts of the image. Since each patch token usually corresponds to one local region of the image, to filter out background noise and focus on related regions, we deploy a set of feature adaptive aggregation (FAA) modules to derive  $p$  relevant local features of  $x^{img}$ , where each FAA module is formulated as follows:

$$\begin{cases} v = agg \otimes F_{patch}^{img} \\ agg = \sigma(Conv(F_{patch}^{img})) \end{cases} \quad (1)$$

where  $Conv(\cdot)$  represents the  $1 \times 1$  convolution layer,  $\sigma(\cdot)$  denotes the sigmoid activation function,  $agg \in \mathbb{R}^n$  is the weight vector, the  $k$ -th element of  $agg$  is the weight for  $k$ -th patch feature.  $\otimes$  represents matrix product, and  $v \in \mathbb{R}^d$  is the local feature obtained by an FAA module. We vertically concatenate the local features produced by  $p$  FAA modules to obtain the local feature matrix  $F_l^{img} \in \mathbb{R}^{p \times d}$ .

**Global features extraction.** Normally, the ViT output of [CLS] token is regarded as containing various global information of the image, which highly entangles both attribute and object features together[8]. To disperse multi-granularity global information into different representa-

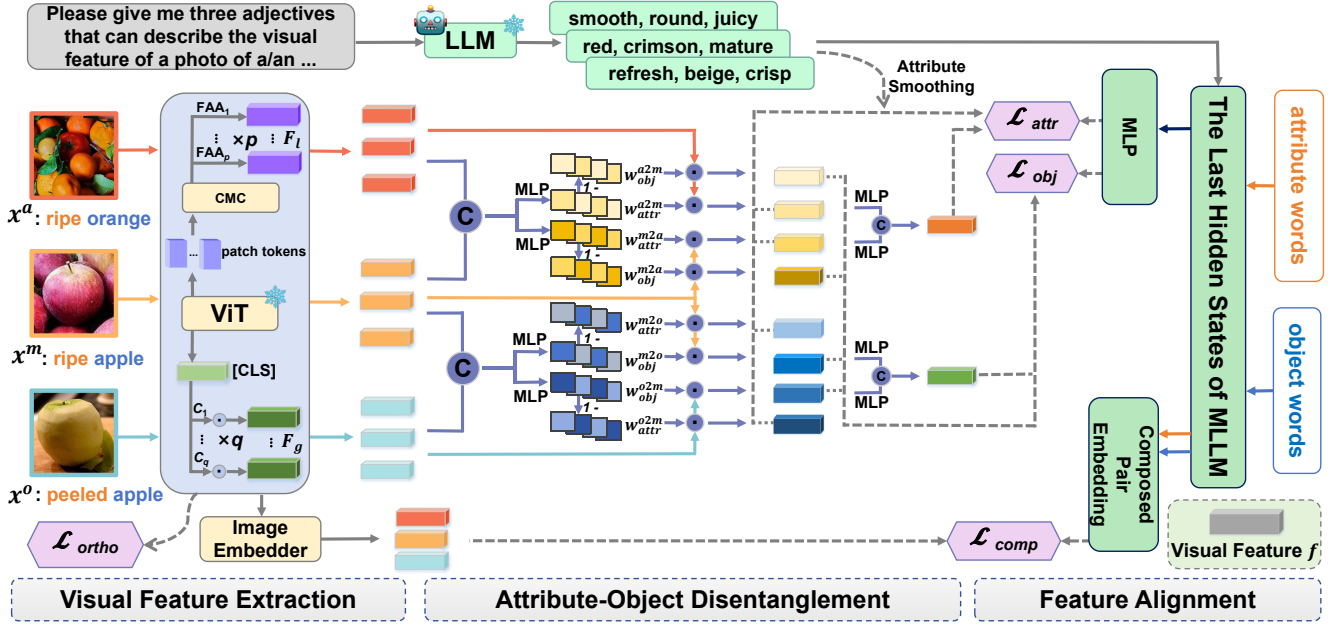


Figure 2. The overall architecture of our proposed **TRIDENT**. **TRIDENT** consists of three major modules: (a) visual feature extraction, (b) attribute-object disentanglement, and (c) feature alignment.

tions,  $q$  learnable condition masks are applied to  $f_{cls}^{img}$  to obtain  $q$  different global representations, where each global representation is computed as:

$$u = f_{cls}^{img} \odot c \quad (2)$$

where  $u \in \mathbb{R}^d$  denotes each global representation. Here  $c \in \mathbb{R}^d$  refers to each learnable condition mask and  $\odot$  is the element-wise multiplication. Consequently, we vertically concatenate  $q$  global representations to derive the global feature matrix  $F_g^{img} \in \mathbb{R}^{q \times d}$ .

**Features concatenation.** Finally,  $F_l^{img}$  and  $F_g^{img}$  are vertically concatenated to form the visual features of  $x^{img}$ , i.e.,  $F^{img} = [F_l^{img}, F_g^{img}] \in \mathbb{R}^{(p+q) \times d}$ , which is used for the following disentanglement of attribute and object.

**Orthogonal regularization.** We ideally want features extracted by different modules can represent different information of the image  $x^{img}$ . To this end, we further introduce the orthogonal regularization, i.e.:

$$\mathcal{L}_{ortho} = \sum_{img \in \{m, a, o\}} (\|F^{img} F^{img^T} - I\|_{Fro}) \quad (3)$$

where  $I \in \mathbb{R}^{(p+q) \times (p+q)}$  is the identity matrix.  $\|\cdot\|_{Fro}$  refers to the Frobenius norm of the matrix.

**Image embedder.** Inspired by [26], for the input image  $x^{img}$ , we first use AveragePools  $Avg(\cdot)$  on  $F_g^{img}$  and  $F_l^{img}$ , respectively, and horizontally concatenate them by  $Cat(\cdot, \cdot)$  to aggregate both global and local visual information of  $x^{img}$  corresponding to the composition label. Then the concatenated feature passes through a linear layer  $Lin_{comp}(\cdot)$

to derive the final feature representation  $f_{comp}^{img}$ . This module is formulated as follows:

$$f_{comp}^{img} = Lin_{comp}(Cat(Avg(F_g^{img}), Avg(F_l^{img}))) \quad (4)$$

where  $f_{comp}^{img} \in \mathbb{R}^{2d}$  denotes the visual feature corresponding to the composition. This module is designed to learn the visual features of images associated with their corresponding composition labels, serving as the primary branch for inference.

### 3.2.2. Attribute-Object Disentanglement

As mentioned before, one of the key challenges for CZSL task is to disentangle attribute and object from visual features. To overcome such challenge, we propose a novel weighted disentanglement module to disentangle primitives, as illustrated in Figure 2. For brevity, one image pair  $x^m$  and  $x^a$  from the triplet image set is taken as an example to elaborate on this module, while another image pair  $x^m$  and  $x^o$  follows the same architecture.

**Weights computation.** The features of  $x^m$  and  $x^a$  (i.e.,  $F^a$  and  $F^o$ ) are vertically concatenated and fed into two MLP modules to derive their respective weights of shared attribute features relative to each other, and subsequently utilize them to compute the weights of their own exclusive object features as follows:

$$\begin{cases} w_{attr}^{m2a} = \sigma(MLP_{m2a}([F^m, F^a])) \\ w_{obj}^{m2a} = 1 - w_{attr}^{m2a} \\ w_{attr}^{a2m} = \sigma(MLP_{a2m}([F^m, F^a])) \\ w_{obj}^{a2m} = 1 - w_{attr}^{a2m} \end{cases} \quad (5)$$

where  $w_{attr}^{m2a}, w_{attr}^{a2m} \in \mathbb{R}^h$  demonstrate the weights of the shared attribute features of  $x^m$  relative to  $x^a$ , and  $x^a$  relative to  $x^m$ , respectively.  $w_{obj}^{m2a}$  and  $w_{obj}^{a2m}$  denote the weights of exclusive object features corresponding to  $x^m$  and  $x^a$ , respectively, which are derived by "1 - shared weights" paradigm as beyond the shared features of the image pair are the exclusive features of each image. Taking  $w_{attr}^{m2a}$  as an example, its  $k$ -th element refers to the shared attribute proportion of  $k$ -th feature of  $x^m$  relative to  $x^a$ .

**Disentangled features obtainment.** We multiply elements of each weight by the corresponding features and then calculate the average. The following takes the process of obtaining the shared attribute features of image  $x^m$  relative to  $x^a$  as an example:

$$f_{attr}^{m2a} = \frac{1}{h} \sum_{i=1}^h w_{attr}^{m2a} F^a_{i,:} \quad (6)$$

where  $F^a_{i,:}$  denotes the  $i$ -th row of  $F^a$ , *i.e.*, the  $i$ -th feature of  $x^a$ .  $w_{attr}^{m2a}$  refers to the  $i$ -th element of  $w_{attr}^{m2a}$ , and  $f_{attr}^{m2a} \in \mathbb{R}^d$  is the shared attribute feature of  $x^m$  relative to  $x^a$ .

For the image pair of  $x^m$  and  $x^a$ , four parts are obtained: the shared attribute features of  $x^m$  relative to  $x^a$ , and  $x^a$  relative to  $x^m$ , as well as two exclusive object features of the image pair, respectively. These four features are marked as  $f_{pri}^e$ , where  $e \in \{m2a, a2m\}$  and  $pri \in \{attr, obj\}$ . Then the shared attribute feature of  $x^a$  and  $x^m$  without relativity is obtained by an MLP layer, which is less dependent on the object. The process is as follows:

$$f_{attr}^{ma} = MLP_{ma}(Cat(f_{attr}^{m2a}, f_{attr}^{a2m})) \quad (7)$$

Similarly, we disentangle attribute and object for  $x^m$  and  $x^o$  and obtain the same features as  $x^m$  and  $x^a$ :  $f_{pri}^e$ , where  $e \in \{m2o, o2m\}$  and  $pri \in \{obj, attr\}$  and  $f_{obj}^{mo}$ .

### 3.2.3. Feature Alignment

Inspired by [24] that leverages the last hidden states as the representation embeddings, we consider the last hidden states of LLaVA v1.5 [16] as our MLLM embeddings for words. Moreover, to tackle the problem that the ineffective overconfidence exhibited by the models in terms of the ground-truth attribute hinders them from generalizing to unseen compositions, GPT 3.5 is employed to generate several auxiliary attributes that describe an object with only one ground-truth attribute and perform label smoothing during attribute alignment. Now we detail each part of feature alignment.

**Generating auxiliary attribute words by LLM.** Since only attribute text needs to be generated, we leverage a LLM, GPT-3.5, instead of MLLM, to generate several auxiliary attributes for each composition. Specifically, the following prompt is input to LLM: 'Please give me  $t$  adjectives that can describe the visual feature of a photo of a/an

... well.', where  $t$  is the number of auxiliary attributes and attribute-object composition (*e.g.*, peeled apple) is filled in '...'. Please refer to Appendix A for more details about the generation of auxiliary attributes by GPT-3.5. Subsequently, the generated auxiliary attribute words form a set  $\mathcal{A}_a$ . Therefore, the set of all words  $\mathcal{Y}$  is obtained, including attributes, objects and auxiliary attributes as follows:

$$\mathcal{Y} = \mathcal{A} \cup \mathcal{O} \cup \mathcal{A}_a \quad (8)$$

**Obtaining MLLM embeddings for words and compositions.** Each word  $y \in \mathcal{Y}$  is fed into LLaVA v1.5 to get the last hidden states, *i.e.*,  $LLaVA_{lhs}(\cdot)$ . Please refer to Appendix B for more details about the obtainment of the last hidden states of LLaVA v1.5 for an input word. Subsequently, they are passed through an MLP layer to get embeddings  $E_{word}(\cdot)$  of aligned dimension with visual features. And for a composed pair  $c$  of attribute  $a$  and object  $o$ , *i.e.*,  $c = (a, o)$ , we get the last hidden states of LLaVA v1.5 for  $a$  and  $o$ , respectively, which are then horizontally concatenated and fed into a linear layer  $Lin_{co}(\cdot)$  to get the composed pair embedding  $E_{co}(\cdot)$ . The process is formulated as follows:

$$E_{word}(y) = MLP_{wd}(LLaVA_{lhs}(y)) \quad (9)$$

$$E_{co}(c) = Lin_{co}(Cat((LLaVA_{lhs}(a), (LLaVA_{lhs}(o)))) \quad (10)$$

**Word expanding.** Prior works compute cosine similarities of disentangled features and word embeddings only within the respective domains of attributes or objects, which results in the disentangled attributes and objects still retaining the information of each other. To address the problem, we propose a word expanding strategy, which computes cosine similarities of visual features and the embeddings of all words, including attributes and objects, and treats all words except the ground-truth word as negative labels.

**Alignment by cross-entropy.** Similar to [19], we use cross-entropy to process the cosine similarity of visual features and word embeddings. Assume that  $f$  is the visual embedding and  $E_{word}(wd)$  is the word embedding for the word  $wd \in \mathcal{Y}$  in a joint space. The classifier logit from  $f$  to  $E_{word}(wd)$  is defined as follows:

$$CE(f, wd) = \frac{e^{\delta \cdot \cos(f, E_{word}(wd))}}{\sum_{y \in \mathcal{Y}} e^{\delta \cdot \cos(f, E_{word}(y))}} \quad (11)$$

where  $\delta$  is the temperature variable, and  $\cos(\cdot, \cdot)$  denotes cosine similarity function. Thus cross-entropy with/without label smoothing can be uniformly formulated as follows:

$$H(f, \mathcal{Y}) = \sum_{y \in \mathcal{Y}} -z \log(CE(f, y))$$

$$\text{with } z = \begin{cases} 1 - \alpha, & \text{if } y \text{ is ground truth label} \\ \alpha/t, & \text{if } y \text{ is auxiliary label} \\ 0, & \text{otherwise} \end{cases} \quad (12)$$

where  $\alpha$  denotes the smoothing factor,  $t$  refers to the number of auxiliary labels and  $z \in [0, 1]$  represents the target value of one-hot or smoothing label. For cross-entropy without label smoothing, *i.e.* with one-hot label  $H_{oh}$ ,  $\alpha$  is set to 0. And the cross-entropy with label smoothing is denoted as  $H_{ls}$ .

For the disentangled attribute features of one image relative to each other, since a single object exhibits multiple attributes, we exploit attribute smoothing with auxiliary attributes to undermine the confidence in the ground-truth attribute and learn more related attributes. For the shared attribute features without relativity, one-hot label is used to compute its classification loss. The loss for disentangled attributes can be defined as follows:

$$\mathcal{L}_{attr} = \sum_{c \in \{m2a, a2m, m2o, o2m\}} H_{ls}(F_{attr}^e, \mathcal{Y}) + H_{oh}(F_{attr}^{ma}, \mathcal{Y}) \quad (13)$$

Concerning the disentangled object features, we use cross-entropy with one-hot label to learn the prototype of the object and the loss is as follows:

$$\mathcal{L}_{obj} = \sum_{c \in \{m2a, a2m, m2o, o2m\}} H_{oh}(F_{obj}^e, \mathcal{Y}) + H_{oh}(F_{obj}^{mo}, \mathcal{Y}) \quad (14)$$

With respect to the visual feature of the image from image embedder, we calculate the cosine similarity between visual embedding and the composed pair embedding of the corresponding composition label and use one-hot label to align them. The classification loss for compositions is as follows:

$$\mathcal{L}_{comp} = \sum_{img \in \{m, a, o\}} H_{oh}(F_{comp}^{img}, \mathcal{C}_s) \quad (15)$$

### 3.3. Training and Inference

During the training phase, the overall loss function is formulated as follows:

$$\mathcal{L} = \gamma_{ortho} \mathcal{L}_{ortho} + \gamma_{comp} \mathcal{L}_{comp} + \gamma_{attr} \mathcal{L}_{attr} + \gamma_{obj} \mathcal{L}_{obj} \quad (16)$$

where  $\gamma_{ortho}$ ,  $\gamma_{comp}$ ,  $\gamma_{attr}$ , and  $\gamma_{obj}$  are weighting factors to balance the influence of different losses.

For inference, we use the composition feature space generated by the classifier that is obtained by optimizing  $\mathcal{L}_{comp}$ . Specifically, given an image from test set, the cosine similarities of its visual feature obtained by image embedder and the composed pair embeddings of all candidate compositions in the test set are computed. The composition with the highest similarity is the class predicted by the model. Note that although the disentanglement branches are not used for inference, they still influence the formation of the composition feature space through their shared visual feature extraction module described in Section 3.2.1.

## 4. Experiment

### 4.1. Experiment Setup

**Datasets.** We evaluate our model on three challenging CZSL benchmark datasets: MIT-states [11], C-GQA [25], and VAW-CZSL [38]. We present the introduction and common data splits of the three datasets in Appendix C.

**Metrics.** Following the common generalized CZSL setting [33], we evaluate our model on seen and unseen pairs separately. Based on them, a calibration bias trades off between the accuracies of seen and unseen pairs. We calculate area under the curve *AUC* (in %) using seen and unseen classification accuracies at different biases in test data. The best seen and unseen accuracies *Seen* and *Unseen* (in %) of the curve are also reported. In addition, we calculate the harmonic mean of seen and unseen classification accuracies at difference biases and report the best one *HM* (in %).

**Implementation details.** We use the visual encoder of LLaVA v1.5, Vit-large-14-336px as our frozen feature extractor, whose outputs contain 577 tokens (1 [CLS] and 576 patch tokens) of 1024 dimensions. The cross-modal connector of LLaVA v1.5 maps the features to the dimension of 4096, the same as last hidden states of based LLM Vicuna v1.5 [45]. Image embedder and the MLP for words map them to the dimension of 1024 for faster training. **TRIDENT** and all baseline models are trained with 128 batch size for 50 epochs. The number of global features is set to 6, 2, 4 for the three datasets, respectively, and the number of local features is twice that of global features. The label smoothing factor is set to 0.09, 0.03, 0.03 for the three datasets, respectively. The number of generated auxiliary attributes for each composition is set to 3. Refer to Appendix D for more information about implementation.

**Baselines.** We compare our **TRIDENT** with recent and prominent approaches in the task of CZSL: SymNet [15], CompCos [19], Co-CGE [20], SCEN [13], OADis [38], INV [44], CANet [42], and ProCC [10]. We replace their backbone with Vit-large-14-336px and retrain all models with the same epoch for the sake of fairness. In addition, although comparing **TRIDENT** with CLIP-based CZSL methods, which rely on the dual-tower architecture, is very unfair due to the significant addition of trainable parameters and training overhead for both the text and visual encoders, we still choose the foundational CLIP and CoOp models as baselines for their strong zero-shot classification abilities.

### 4.2. Results and Discussion

In this section, we compare **TRIDENT** with state-of-the-art methods. As shown in Table 1, **TRIDENT** surpasses other models by a substantial margin in general. For MIT-States, **TRIDENT** boosts *AUC*, *HM*, and *Unseen* from 13.6%, 29.8%, and 39.9% of CANet to the new state-of-the-art performance of 14.2%, 30.9%, and 40.0% with 0.6%,

| Method                | MIT-States  |             |             |               | C-GQA      |             |             |               | VAW-CZSL   |             |             |               |
|-----------------------|-------------|-------------|-------------|---------------|------------|-------------|-------------|---------------|------------|-------------|-------------|---------------|
|                       | <i>AUC</i>  | <i>HM</i>   | <i>Seen</i> | <i>Unseen</i> | <i>AUC</i> | <i>HM</i>   | <i>Seen</i> | <i>Unseen</i> | <i>AUC</i> | <i>HM</i>   | <i>Seen</i> | <i>Unseen</i> |
| SymNet [15]           | 3.2         | 13.7        | 22.7        | 20.1          | 1.9        | 10.8        | 20.3        | 11.8          | 2.8        | 13.5        | 20.2        | 18.0          |
| CompCos [19]          | 12.3        | 28.2        | 39.0        | 39.5          | 5.0        | 17.7        | 32.8        | 19.1          | 6.5        | 20.8        | 30.5        | 27.4          |
| Co-CGE [20]           | 10.3        | 25.1        | 41.0        | 33.1          | 4.2        | 15.2        | 32.9        | 17.0          | 6.2        | 19.7        | 31.0        | 26.1          |
| SCEN [13]             | 9.8         | 24.6        | 35.1        | 36.5          | 3.8        | 15.3        | 31.5        | 15.7          | 5.7        | 19.2        | 29.9        | 24.5          |
| OADis [38]            | 13.1        | 29.0        | 42.3        | 27.3          | 2.3        | 12.1        | 23.3        | 12.8          | 4.1        | 16.2        | 26.0        | 20.7          |
| INV [44]              | 11.5        | 26.6        | 28.5        | 25.0          | 1.4        | 7.9         | 28.6        | 6.8           | 2.0        | 11.1        | 21.1        | 11.9          |
| CANet [42]            | <u>13.6</u> | <u>29.8</u> | <b>46.4</b> | 39.9          | <u>5.7</u> | <u>18.9</u> | <u>34.8</u> | 20.5          | <u>6.7</u> | <u>21.0</u> | <u>31.2</u> | <u>27.4</u>   |
| ProCC [10]            | 9.5         | 28.1        | 43.1        | 39.1          | 3.5        | 15.1        | 32.4        | 15.8          | 3.6        | 18.9        | 26.9        | 25.5          |
| CLIP [28]             | 11.0        | 26.1        | 30.2        | <u>46.0</u>   | 1.4        | 8.6         | 7.5         | <u>25.0</u>   | -          | -           | -           | -             |
| CoOp [28]             | 13.5        | 29.8        | 34.4        | <b>47.6</b>   | 4.4        | 17.1        | 20.5        | <b>26.8</b>   | -          | -           | -           | -             |
| <b>TRIDENT (Ours)</b> | <b>14.2</b> | <b>30.9</b> | <u>44.5</u> | 40.0          | <b>8.0</b> | <b>22.6</b> | <b>39.5</b> | 24.1          | <b>8.3</b> | <b>23.4</b> | <b>33.3</b> | <b>31.1</b>   |

Table 1. Comparison with the state-of-the-art results on MIT-States, C-GQA and VAW-CZSL. We compare our **TRIDENT** with the state-of-the-art methods on test *AUC*, best seen (*Seen*), best unseen (*Unseen*) and best harmonic mean (*HM*) accuracies on these three datasets. We measure top-1 *AUC* on MIT-States and C-GQA, and top-3 *AUC* on VAW-CZSL. Best results are displayed in **boldface**, and second best results are underlined.

1.1%, and 0.1% improvement, respectively. Our model achieves competitive performance on MIT-States benchmark, despite considerable label noise [2]. However, for the more challenging benchmark C-GQA, **TRIDENT** achieves 8.0%, 22.6%, 39.5%, and 24.1% on the metrics of *AUC*, *HM*, *Seen*, and *Unseen*, providing 2.3%, 3.7%, 4.7%, and 3.6% improvements on the previous state-of-the-art model CANet. For the existing most challenging benchmark dataset VAW-CZSL, **TRIDENT** attains performance of 8.3%, 23.4%, 23.4%, and 33.3%, surpassing CANet by 1.6%, 2.4%, 2.2%, and 3.7% in terms of *AUC*, *HM*, *Seen*, and *Unseen*. The largest improvement is observed in the *Unseen* metric, indicating that attribute smoothing helps enhance the generalization ability of the model. We observe **TRIDENT** performs significantly better than CANet regarding all metrics on two challenging and low-noise benchmark dataset C-GQA and VAW-CZSL, indicating the efficacy of our approach. This improvement arises from the utilization of MLLM embeddings and attribute smoothing, which enhance attribute-object disentanglement and consequently facilitate the recognition of unseen compositions while maintaining performance on seen compositions.

In addition, we compare **TRIDENT** with dual-tower CLIP and CoOp after fine-tuned for the CZSL task. Since they are trained on a large amount of image-text data, they possess zero-shot image classification capabilities, which leads to better classification results for unseen images. Regarding *Unseen* metric, CoOp outperforms **TRIDENT** by 7.6% and 2.7% on MIT-States and C-GQA, respectively. However, **TRIDENT** surpasses CoOp by 0.7% and 1.1% on the core metrics of *AUC* and *HM* on MIT-States, as well as 3.6% and 5.5% on C-GQA, which suggests **TRIDENT** performs better than CLIP and CoOp in CZSL task.

### 4.3. Ablation Study

**Effectiveness of each component.** We ablate certain module of **TRIDENT** to evaluate the contribution of each mod-

| Method   | <i>AUC</i>  | <i>HM</i>   | <i>Seen</i> | <i>Unseen</i> |
|--|-------------|-------------|-------------|---------------|
| <i>w/o condition_masks</i>                                     | 14.0        | 30.5        | 44.2        | 39.8          |
| <i>w/o FAAs</i>  | 13.9        | 30.4        | 44.4        | 39.7          |
| <i>w/o word_expanding</i>                                      | 14.0        | 30.1        | 44.7        | 39.8          |
| <i>w/o attribute_smoothing</i>                                 | 13.9        | 30.5        | <b>44.9</b> | 39.5          |
| <i>w/o <math>\mathcal{L}_{attr} + \mathcal{L}_{obj}</math></i> | 13.2        | 30.1        | 43.8        | 38.9          |
| <i>w/o <math>\mathcal{L}_{ortho}</math></i>                    | 14.1        | 30.7        | 44.6        | 39.7          |
| <b>TRIDENT</b>   | <b>14.2</b> | <b>30.9</b> | 44.5        | <b>40.0</b>   |

Table 2. Ablation study results on MIT-States. *w/o certain\_part* denotes this part is ablated.

ule on MIT-States, as it is the most common used dataset. The ablation results are reported in Table 2. From this table, we gain the following observations.

1) Both *w/o condition\_masks* model and *w/o FAAs* model perform worse than **TRIDENT**, which validates the importance of extracting the multi-granularity features and filtering out the background noise, respectively.

2) **TRIDENT** surpasses *w/o word\_expanding* model and *w/o attribute\_smoothing* model on the *Unseen* metric, yet falls short of them on the *Seen* metric. The difference between **TRIDENT** and the *w/o word\_expanding* model stems from its more thorough disentanglement, which enhances the recognition of unseen images while weakens the identification of seen images. The disparity between **TRIDENT** and the *w/o attribute\_smoothing* model arises from attribute smoothing, which diminishes the confidence of the model in seen compositions, facilitating its generalization to unseen compositions. However, the improvement of **TRIDENT** over these two models on *AUC* and *HM* indicates the effectiveness of word expanding and label smoothing strategy.

3) **TRIDENT** outperforms *w/o  $\mathcal{L}_{attr} + \mathcal{L}_{obj}$*  model on all metrics, confirming that the attribute-object disentanglement module is highly advantageous for generalization from seen compositions to unseen compositions.

4) *w/o  $\mathcal{L}_{ortho}$*  model is inferior to **TRIDENT**, which



(a) image-to-text retrieval. (b) text-to-image retrieval (successful cases). (c) text-to-image retrieval (failure cases).

Figure 3. Qualitative analysis. (a) Top-5 image-to-text retrieval cases. The first two rows display successful cases, while the last row presents failure cases. (b) Successful cases of top-5 text-to-image retrieval. (c) Failure cases of top-5 text-to-image retrieval. In all cases, the attribute and object of composition label are marked in orange and blue, respectively. And the successful and failure retrieval results are tagged in green and red, respectively.

| Method         | <i>Vari-ent</i> | <i>AUC</i>  | <i>HM</i>   |
|----------------|-----------------|-------------|-------------|
| SCEN [13]      | $ft+w2v$        | 8.2         | 22.8        |
|                | $LLaVA_{lhs}$   | <b>10.3</b> | <b>25.1</b> |
| CANet [42]     | $ft+w2v$        | 12.3        | <b>28.4</b> |
|                | $LLaVA_{lhs}$   | <b>12.5</b> | 28.3        |
| <b>TRIDENT</b> | $ft+w2v$        | 14.0        | 29.9        |
|                | $LLaVA_{lhs}$   | <b>14.2</b> | <b>30.9</b> |

Table 3. Impact of word embedding on MIT-States.  $ft + w2v$  means the sum of Word2Vec and Fasttext.  $LLaVA_{lhs}$  represents the last hidden states of LLaVA v1.5.

suggests the designed orthogonal regularization is helpful to guarantee different features extract different information.

**Impact of word embeddings.** Our work leverages the last hidden states of LLaVA v1.5 ( $LLaVA_{lhs}$ ) as word embeddings, while Word2Vec [21] and Fasttext [3] are the most common word embeddings for MIT-States in previous works. In Table 3, based on three models: SCEN [13], CANet [42] and **TRIDENT**, we compare the performance of employing the last hidden states of LLaVA v1.5 and the sum of Word2Vec and Fasttext ( $ft+w2v$ ), respectively. The results indicate that the last hidden states of MLLM capture more complex multimodal semantic information than ordinary word embeddings.

For details on the impact of hyperparameters, including the number of visual features and the label smoothing factor, please refer to Appendix E.

#### 4.4. Qualitative Analysis

Inspired by [8], we use **TRIDENT** to conduct both image-to-text retrieval and text-to-image retrieval experiments on the three datasets. We first consider image-to-text retrieval, shown in Figure 3a. The first two rows display successful cases, while the last row presents failure cases. And the cases shown in these three columns are drawn from the three datasets, respectively. Given an image, such as the image of burnt house, we extract its visual features by image embedder and retrieve the top-5 closest composed pair embeddings of compositions. For successful cases, such as the

image labeled burnt house, we notice that the top four predictions can both describe logs burning on fire in the image. In terms of the image labeled green leaf, another successful case, the predicted attributes can also describe leaf, which is thanks to attribute smoothing learning more attributes for an object. For the failure cases, such as the image labeled multicolored teddy-bear, the model focuses on the main orange bear and neglects the multicolored background, which is attributed to FAA modules.

We then consider text-to-image retrieval. Successful cases are shown in Figure 3b, while failure cases are shown in Figure 3c. Given a text composition, we embed it and retrieve the top-5 closest images. We observe that the retrieved images of peeled orange are definitely correct. However, the retrieved images of green grapes are all wrong. This is due to the fact that the training images of green grapes in C-GQA dataset are almost filled with a single grape, making it difficult for the model to capture the contour features of a bunch of green grapes. The image-to-text and text-to-image retrieval experiments confirm that our model effectively projects visual features and word embeddings into a unified space.

## 5. Conclusion

In this work, we propose a novel framework termed **TRIDENT** to address the challenging CZSL task. First, we leverage feature adaptive aggregation modules to mitigate the impact of background, and utilize learnable condition masks to capture multi-granularity features for attribute-object disentanglement. In addition, we exploit the last hidden states of MLLM to replace ordinary word embeddings, as they can capture complex multimodal semantic information. Moreover, we leverage LLM to generate auxiliary attributes and perform attribute smoothing to diminish overconfidence of models in seen compositions, which enables models to generalize to unseen compositions better. Extensive experiments have been conducted on three challenging datasets, and the results demonstrate the effectiveness of **TRIDENT**. In the future, we plan to extend our method to harness the powerful capabilities of LLMs, MLLMs, and CLIP to more effectively address the CZSL task.



## References

- [1] Jean-Baptiste Alayrac, Jeff Donahue, Pauline Luc, Antoine Miech, Iain Barr, Yana Hasson, Karel Lenc, Arthur Mensch, Katherine Millican, Malcolm Reynolds, Roman Ring, Eliza Rutherford, Serkan Cabi, Tengda Han, Zhitao Gong, Sina Samangooei, Marianne Monteiro, Jacob L Menick, Sebastian Borgeaud, Andy Brock, Aida Nematzadeh, Sahand Sharifzadeh, Mikolaj Binkowski, Ricardo Barreira, Oriol Vinyals, Andrew Zisserman, and Karén Simonyan. Flamingo: a visual language model for few-shot learning. In *Advances in Neural Information Processing Systems*, pages 23716–23736, 2022. 3
- [2] Yuval Atzmon, Felix Kreuk, Uri Shalit, and Gal Chechik. A causal view of compositional zero-shot recognition. In *Advances in Neural Information Processing Systems*, pages 1462–1473, 2020. 7
- [3] Piotr Bojanowski, Edouard Grave, Armand Joulin, and Tomas Mikolov. Enriching word vectors with subword information. *Transactions of the Association for Computational Linguistics*, 5:135–146, 2017. 8
- [4] Tom Brown, Benjamin Mann, Nick Ryder, Melanie Subbiah, Jared D Kaplan, Prafulla Dhariwal, Arvind Neelakantan, Pranav Shyam, Girish Sastry, Amanda Askell, Sandhini Agarwal, Ariel Herbert-Voss, Gretchen Krueger, Tom Henighan, Rewon Child, Aditya Ramesh, Daniel Ziegler, Jeffrey Wu, Clemens Winter, Chris Hesse, Mark Chen, Eric Sigler, Mateusz Litwin, Scott Gray, Benjamin Chess, Jack Clark, Christopher Berner, Sam McCandlish, Alec Radford, Ilya Sutskever, and Dario Amodei. Language models are few-shot learners. In *Advances in Neural Information Processing Systems*, pages 1877–1901, 2020. 3
- [5] Wei-Lin Chiang, Zhuohan Li, Zi Lin, Ying Sheng, Zhanghao Wu, Hao Zhang, Lianmin Zheng, Siyuan Zhuang, Yonghao Zhuang, Joseph E. Gonzalez, Ion Stoica, and Eric P. Xing. Vicuna: An open-source chatbot impressing gpt-4 with 90%\* chatgpt quality, 2023. 3
- [6] Jacob Devlin, Ming-Wei Chang, Kenton Lee, and Kristina Toutanova. BERT: Pre-training of deep bidirectional transformers for language understanding. In *Proceedings of the Conference of the North American Chapter of the Association for Computational Linguistics: Human Language Technologies, Volume 1 (Long and Short Papers)*, pages 4171–4186, 2019. 2
- [7] Alexey Dosovitskiy. An image is worth 16x16 words: Transformers for image recognition at scale. *arXiv preprint arXiv:2010.11929*, 2020. 3
- [8] Shaozhe Hao, Kai Han, and Kwan-Yee K. Wong. Learning attention as disentangler for compositional zero-shot learning. In *Proceedings of the IEEE/CVF Conference on Computer Vision and Pattern Recognition*, pages 15315–15324, 2023. 1, 3, 8
- [9] Siteng Huang, Biao Gong, Yutong Feng, Min Zhang, Yiliang Lv, and Donglin Wang. Troika: Multi-path cross-modal traction for compositional zero-shot learning. In *Proceedings of the IEEE/CVF Conference on Computer Vision and Pattern Recognition*, pages 24005–24014, 2024. 2
- [10] Fushuo Huo, Wenchao Xu, Song Guo, Jingcai Guo, Haozhao Wang, Ziming Liu, and Xiaocheng Lu. Procc: Progressive cross-primitive compatibility for open-world compositional zero-shot learning. In *Proceedings of the AAAI Conference on Artificial Intelligence*, pages 12689–12697, 2024. 6, 7
- [11] Phillip Isola, Joseph J Lim, and Edward H Adelson. Discovering states and transformations in image collections. In *Proceedings of the IEEE Conference on Computer Vision and Pattern Recognition*, pages 1383–1391, 2015. 6, 12
- [12] Jing Yu Koh, Ruslan Salakhutdinov, and Daniel Fried. Grounding language models to images for multimodal inputs and outputs. In *Proceedings of the International Conference on Machine Learning*, pages 17283–17300, 2023. 2, 3
- [13] Xiangyu Li, Xu Yang, Kun Wei, Cheng Deng, and Muli Yang. Siamese contrastive embedding network for compositional zero-shot learning. In *Proceedings of the IEEE/CVF Conference on Computer Vision and Pattern Recognition*, pages 9326–9335, 2022. 2, 6, 7, 8
- [14] Xiangyu Li, Xu Yang, Xi Wang, and Cheng Deng. Agree to disagree: Exploring partial semantic consistency against visual deviation for compositional zero-shot learning. *IEEE Transactions on Cognitive and Developmental Systems*, 16(4):1433–1444, 2024. 1
- [15] Yong-Lu Li, Yue Xu, Xiaohan Mao, and Cewu Lu. Symmetry and group in attribute-object compositions. In *Proceedings of the IEEE/CVF Conference on Computer Vision and Pattern Recognition*, page 11313–11322, 2020. 2, 6, 7
- [16] Haotian Liu, Chunyuan Li, Yuheng Li, and Yong Jae Lee. Improved baselines with visual instruction tuning. In *Proceedings of the IEEE/CVF Conference on Computer Vision and Pattern Recognition*, pages 26296–26306, 2024. 2, 3, 5
- [17] Haotian Liu, Chunyuan Li, Qingyang Wu, and Yong Jae Lee. Visual instruction tuning. *Advances in neural information processing systems*, 36, 2024. 3
- [18] Xiaocheng Lu, Song Guo, Ziming Liu, and Jingcai Guo. Decomposed soft prompt guided fusion enhancing for compositional zero-shot learning. In *Proceedings of the IEEE/CVF Conference on Computer Vision and Pattern Recognition*, pages 23560–23569, 2023. 2
- [19] Massimiliano Mancini, Muhammad Ferjad Naeem, Yongqin Xian, and Zeynep Akata. Open world compositional zero-shot learning. In *Proceedings of the IEEE/CVF Conference on Computer Vision and Pattern Recognition*, pages 5222–5230, 2021. 5, 6, 7
- [20] Massimiliano Mancini, Muhammad Ferjad Naeem, Yongqin Xian, and Zeynep Akata. Learning graph embeddings for open world compositional zero-shot learning. *IEEE Transactions on Pattern Analysis and Machine Intelligence*, 46(3): 1545–1560, 2022. 2, 6, 7
- [21] Tomas Mikolov. Efficient estimation of word representations in vector space. *arXiv preprint arXiv:1301.3781*, 2013. 2, 8
- [22] Ishan Misra, Abhinav Gupta, and Martial Hebert. From red wine to red tomato: Composition with context. In *Proceedings of the IEEE Conference on Computer Vision and Pattern Recognition*, pages 1160–1169, 2017. 1
- [23] Niklas Muennighoff. Sgpt: Gpt sentence embeddings for semantic search. *arXiv preprint arXiv:2202.08904*, 2022. 2, 3

- [24] Niklas Muennighoff, Hongjin Su, Liang Wang, Nan Yang, Furu Wei, Tao Yu, Amanpreet Singh, and Douwe Kiela. Generative representational instruction tuning. *arXiv preprint arXiv:2402.09906*, 2024. 2, 3, 5, 12
- [25] Muhammad Ferjad Naem, Yongqin Xian, Federico Tombari, and Zeynep Akata. Learning graph embeddings for compositional zero-shot learning. In *Proceedings of the IEEE/CVF Conference on Computer Vision and Pattern Recognition*, pages 953–962, 2021. 6, 12
- [26] Tushar Nagarajan and Kristen Grauman. Attributes as operators: Factorizing unseen attribute-object compositions. In *Proceedings of the European Conference on Computer Vision*, pages 169–185, 2018. 1, 4
- [27] Zhixiong Nan, Yang Liu, Nanning Zheng, and Song-Chun Zhu. Recognizing unseen attribute-object pair with generative model. In *Proceedings of the AAAI Conference on Artificial Intelligence*, pages 8811–8818, 2019. 1
- [28] Nihal V. Nayak, Peilin Yu, and Stephen H. Bach. Learning to compose soft prompts for compositional zero-shot learning. In *International Conference on Learning Representations*, 2023. 2, 7
- [29] OpenAI. Gpt-3.5-turbo api, 2023. 2
- [30] Long Ouyang, Jeffrey Wu, Xu Jiang, Diogo Almeida, Carroll Wainwright, Pamela Mishkin, Chong Zhang, Sandhini Agarwal, Katarina Slama, Alex Ray, John Schulman, Jacob Hilton, Fraser Kelton, Luke Miller, Maddie Simens, Amanda Askell, Peter Welinder, Paul F Christiano, Jan Leike, and Ryan Lowe. Training language models to follow instructions with human feedback. In *Advances in Neural Information Processing Systems*, pages 27730–27744, 2022. 3
- [31] Adam Paszke, Sam Gross, Francisco Massa, Adam Lerer, James Bradbury, Gregory Chanan, Trevor Killeen, Zeming Lin, Natalia Gimelshein, Luca Antiga, Alban Desmaison, Andreas Kopf, Edward Yang, Zachary DeVito, Martin Raison, Alykhan Tejani, Sasank Chilamkurthy, Benoit Steiner, Lu Fang, Junjie Bai, and Soumith Chintala. Pytorch: An imperative style, high-performance deep learning library. In *Advances in Neural Information Processing Systems*, 2019. 13
- [32] Jeffrey Pennington, Richard Socher, and Christopher Manning. GloVe: Global vectors for word representation. In *Proceedings of the Conference on Empirical Methods in Natural Language Processing*, pages 1532–1543, 2014. 1, 2
- [33] Senthil Purushwalkam, Maximilian Nickel, Abhinav Gupta, and Marc’Aurelio Ranzato. Task-driven modular networks for zero-shot compositional learning. In *Proceedings of the IEEE/CVF International Conference on Computer Vision*, pages 3592–3601, 2019. 1, 3, 6
- [34] Alec Radford, Jeff Wu, Rewon Child, David Luan, Dario Amodei, and Ilya Sutskever. Language models are unsupervised multitask learners, 2019. 2
- [35] Alec Radford, Jong Wook Kim, Chris Hallacy, Aditya Ramesh, Gabriel Goh, Sandhini Agarwal, Girish Sastry, Amanda Askell, Pamela Mishkin, Jack Clark, Gretchen Krueger, and Ilya Sutskever. Learning transferable visual models from natural language supervision. In *Proceedings of the International Conference on Machine Learning*, pages 8748–8763, 2021. 2
- [36] Frank Ruis, Gertjan Burghouts, and Doina Bucur. Independent prototype propagation for zero-shot compositionality. In *Advances in Neural Information Processing Systems*, pages 10641–10653, 2021. 1
- [37] Pranab Sahoo, Ayush Kumar Singh, Sriparna Saha, Vinija Jain, Samrat Mondal, and Aman Chadha. A systematic survey of prompt engineering in large language models: Techniques and applications. *arXiv preprint arXiv:2402.07927*, 2024. 11
- [38] Nirat Saini, Khoi Pham, and Abhinav Shrivastava. Disentangling visual embeddings for attributes and objects. In *Proceedings of the IEEE/CVF Conference on Computer Vision and Pattern Recognition*, pages 13658–13667, 2022. 1, 2, 6, 7, 12
- [39] Justyna Sarzynska-Wawer, Aleksander Wawer, Aleksandra Pawlak, Julia Szymanowska, Izabela Stefaniak, Michal Jarkiewicz, and Lukasz Okruszek. Detecting formal thought disorder by deep contextualized word representations. *Psychiatry Research*, 304:114135, 2021. 2
- [40] Hugo Touvron, Thibaut Lavril, Gautier Izacard, Xavier Martinet, Marie-Anne Lachaux, Timothée Lacroix, Baptiste Rozière, Naman Goyal, Eric Hambro, Faisal Azhar, et al. Llama: Open and efficient foundation language models. *arXiv preprint arXiv:2302.13971*, 2023. 3
- [41] Bin Wang and C.-C. Jay Kuo. Sbert-wk: A sentence embedding method by dissecting bert-based word models. *IEEE/ACM Transactions on Audio, Speech, and Language Processing*, 28:2146–2157, 2020. 2
- [42] Qingsheng Wang, Lingqiao Liu, Chenchen Jing, Hao Chen, Guoqiang Liang, Peng Wang, and Chunhua Shen. Learning conditional attributes for compositional zero-shot learning. In *Proceedings of the IEEE/CVF Conference on Computer Vision and Pattern Recognition*, pages 11197–11206, 2023. 2, 6, 7, 8
- [43] Shuo Xu, Sai Wang, Xinyue Hu, Yutian Lin, Bo Du, and Yu Wu. Mac: A benchmark for multiple attributes compositional zero-shot learning. *arXiv preprint arXiv:2406.12757*, 2024. 2
- [44] Tian Zhang, Kongming Liang, Ruoyi Du, Xian Sun, Zhanyu Ma, and Jun Guo. Learning invariant visual representations for compositional zero-shot learning. In *Proceedings of the European Conference on Computer Vision*, pages 339–355, 2022. 1, 6, 7
- [45] Lianmin Zheng, Wei-Lin Chiang, Ying Sheng, Siyuan Zhuang, Zhanghao Wu, Yonghao Zhuang, Zi Lin, Zhuohan Li, Dacheng Li, Eric Xing, Hao Zhang, Joseph E Gonzalez, and Ion Stoica. Judging llm-as-a-judge with mt-bench and chatbot arena. In *Advances in Neural Information Processing Systems*, pages 46595–46623, 2023. 3, 6
- [46] Kaiyang Zhou, Jingkang Yang, Chen Change Loy, and Ziwei Liu. Conditional prompt learning for vision-language models. In *Proceedings of the IEEE/CVF Conference on Computer Vision and Pattern Recognition*, pages 16816–16825, 2022. 2

## Appendix

### A. Auxiliary Attributes Generation by LLM and Post-process

As mentioned before, we leverage GPT-3.5 to generate some auxiliary attributes for attribute smoothing. The auxiliary attributes are generated based on the contextual composition of the object and its attribute, such as `ripe apple` or `sliced apple`. The model takes into account the unique characteristics that arise from the combination of attribute and the object’s context. This ensures that the auxiliary attributes accurately capture the nuances of the specific composition, rather than general object-level attributes. Since the generation ability of LLM is affected by many factors, in this section, we first explore the impact of different prompts on LLM-generated content. Then we study on the influence of the number of auxiliary attributes  $t$ . In addition, we introduce post-processing of generated text to eliminate potential noise.

**Impact of prompt input to LLM.** Users typically interact with LLMs through prompts to request answers to questions, generate text, complete tasks, and more. The model generates text based on the provided prompt, striving to meet the user’s requirements [37]. Therefore, the good design of prompt is significant for stimulating knowledge of LLMs, which enables them to better follow our instructions and generate auxiliary attributes with high qual-

|          |  |
|----------|--|
| User:    | Please give me five adjectives that are most likely to describe the browned beef well.   |
| GPT-3.5: | 1. Flavorful 2. Juicy 3. Savory 4. Tender 5. Rich  |
| User:    | Now I give you an adjective: browned beef. Please give me five more possible adjectives that can describe the browned beef well. |
| GPT-3.5: | 1. Juicy beef 2. Tender beef 3. Flavorful beef 4. Savory beef 5. Succulent beef  |
| User:    | Please give me five common adjectives that can describe a browned beef well.   |
| GPT-3.5: | 1. Juicy 2. Brown 3. Savory 4. Tender 5. Succulent   |
| User:    | Please give me five adjectives that can describe the visual feature of a photo of a/an browned beef well.                        |
| GPT-3.5: | 1. Juicy 2. Glistening 3. Crispy 4. Sizzling 5. Mouthwatering  |

Table 4. Example prompts with the composition `browned beef` input to GPT-3.5 and the generated text.

|          |   |
|----------|---|
| User:    | Please give me five adjectives that are most likely to describe the inflated pool well.   |
| GPT-3.5: | 1. Spacious 2. Durable 3. Sturdy 4. Bright 5. Relaxing  |
| User:    | Now I give you an object with an adjective: inflated pool. Please give me five more possible adjectives that can describe the inflated pool well. |
| GPT-3.5: | 1. Refreshing inflated pool 2. Relaxing inflated pool 3. Blue inflated pool 4. Large inflated pool 5. Fun inflated pool                           |
| User:    | Please give me five common adjectives that can describe a inflated pool well.   |
| GPT-3.5: | 1. Large 2. Round 3. Inviting 4. Fun 5. Sturdy  |
| User:    | Please give me five adjectives that can describe the visual feature of a photo of a/an inflated pool well.  |
| GPT-3.5: | 1. Colorful 2. Refreshing 3. Sparkling 4. Bright 5. Relaxing  |

Table 5. Example prompts with the composition `inflated pool` input to GPT-3.5 and the generated text.

ity. We first design some prompts with different style, then input them into GPT-3.5 and observe the quality of generated attributes. Some prompt examples on the composition `browned beef` and `ancient building` are shown in Table 4 and Table 5, respectively.

As shown in Table 4, the prompt without “the visual feature of ...” may cause the model to produce adjectives that are not specific but generic, such `Savory` and `Rich`. In both Table 4 and Table 5, the prompts starting with “Now I give you...”, compared to those starting with “Please give me ...”, result in a weaker instruction following ability of the model. Therefore, we choose the prompt: “Please give me five adjectives that can describe the visual feature of a photo of a/an ... well.”

**Impact of the number of auxiliary attributes  $t$ .** In Table 4, we observe that the generated attributes describe the compositions to varying degrees, with later items in the sequence being less relevant generally. Therefore, we study on the influence of the number of auxiliary attributes  $t$ .

Table 7 and Table 8 show the generated text using different  $t$  of compositions `large garden` and `young girl`. The results demonstrate that the greater the number, the more generic adjectives with irrelevant information are included, for example, `Captivating` is generated for both compositions. In addition, with  $t$  increasing, the noise in the generated text due to the uncertainty of the model

| Dataset         | Composition     |                 |                                    | Train             |                 | Validation        |                   |                 | Test              |                   |                 |
|-----------------|-----------------|-----------------|------------------------------------|-------------------|-----------------|-------------------|-------------------|-----------------|-------------------|-------------------|-----------------|
|                 | $ \mathcal{A} $ | $ \mathcal{O} $ | $ \mathcal{A} \times \mathcal{O} $ | $ \mathcal{C}_s $ | $ \mathcal{X} $ | $ \mathcal{C}_s $ | $ \mathcal{C}_u $ | $ \mathcal{X} $ | $ \mathcal{C}_s $ | $ \mathcal{C}_u $ | $ \mathcal{X} $ |
| MIT-States [11] | 115             | 245             | 28175                              | 1262              | 30338           | 300               | 300               | 10420           | 400               | 400               | 12995           |
| C-GQA [25]      | 413             | 674             | 278362                             | 5592              | 26920           | 1252              | 1040              | 7280            | 888               | 923               | 5098            |
| VAW-CZSL [38]   | 440             | 541             | 238040                             | 11175             | 72203           | 2121              | 2322              | 9524            | 2449              | 2470              | 10856           |

Table 6. Summary statistics of the datasets used in our experiments.

|     |   |
|-----|---|
| $t$ | the generated text for the composition<br>large garden  |
| 3   | 1. Lush 2. Vibrant 3. Flourishing   |
| 5   | 1. Lush 2. Expansive 3. Vibrant 4. Serene<br>5. Verdant   |
| 10  | 1. Lush 2. Vibrant 3. Expansive 4. Serene<br>5. Colorful 6. Beautiful 7. Bountiful 8.<br>Captivating 9. Peaceful 10. Tranquil |

Table 7. Impact of  $t$  on the generated text with the composition `large garden`. Note that the input prompt provided to GPT-3.5 is the previously selected one, replacing  $t$  and the composition.

|     |   |
|-----|---|
| $t$ | the generated text for the composition<br>young girl  |
| 3   | 1. Innocent 2. Radiant 3. Youthful  |
| 5   | 1. Youthful 2. Innocent 3. Vibrant 4. Ra-<br>diant 5. Captivating   |
| 10  | 1. Radiant 2. Innocent 3. Vibrant 4. Capti-<br>vating 5. Playful 6. Ethereal 7. Alluring 8.<br>Charming 9. Enchanting 10. Happy |

Table 8. Impact of  $t$  on the generated text with the composition `young girl`. Note that the input prompt provided to GPT-3.5 is the previously selected one, replacing  $t$  and the composition.

about the given image grows. The `young girl` may not be happy, yet the model fails to find ten words to describe her, so it has to guess. Therefore, we set  $t$  to 3, this minimizes the general adjectives and noise while retaining useful information.

**Post-processing of generated text.** GPT-3.5 generates a segment of text, which we need to process into multiple useful words by exploiting regular expressions. However, the auxiliary attributes generated by LLM may contain the attribute of the input composition, for example, generating `ancient` for `ancient building`. At this point, we reuse the model to generate  $t + 1$  adjectives for this composition and select three adjectives that are not the attribute of the input composition.

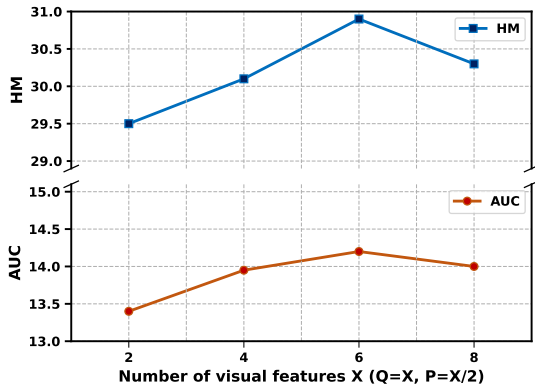
## B. Obtainment of The Last Hidden States of MLLM

We input the attribute (object) word into LLaVA v1.5, which first tokenizes the word into  $z$  tokens. These tokens pass through all attention blocks in the MLLM, ultimately generating  $z$  embeddings of dimension  $d_m$  after the last block, named the last hidden states. Subsequently, we apply average pooling to these  $z$  embeddings of dimension  $d_m$  to obtain a  $d_m$ -dimensional embedding that represents the attribute. Since the last hidden states are designed to generate the next token rather than for representation, Muennighoff et al. [24] leverages instruction to fine-tune the model. Therefore, we fine-tune the last hidden states with a low learning rate during the training phase of **TRIDENT**.

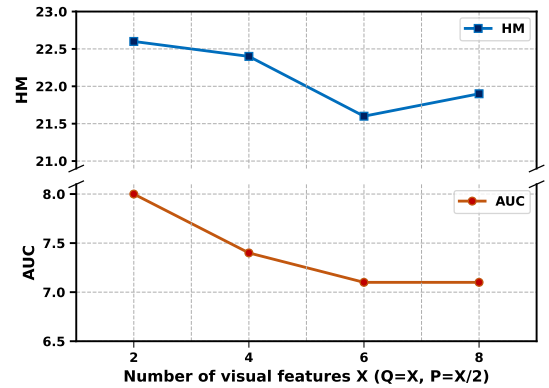
It is important to note that although LLaVA v1.5 may have seen certain images during training, the model is asked to generate textual descriptions of images in an autoregressive manner during training. The textual descriptions focus on the main content of the image, rather than the "attribute-object" label. Therefore, there is no issue of data leakage when training **TRIDENT**.

## C. Data Statistics

We evaluate our model on three challenging CZSL benchmark datasets: MIT-states [11], C-GQA [25], and VAW-CZSL [38]. MIT-states consists of diverse real-world images labeled by early image search engine technology. C-GQA and VAW-CZSL are two more challenging benchmark datasets that consist of broad collections of in-the-wild images. C-GQA has more one-to-one compositions, while objects in VAW-CZSL share more attributes. Table 6 shows detailed data statistics following the common data splits of MIT-States [11], C-GQA [25] and VAW-CZSL [38]. MIT-States contains 53753 images, with 115 attributes and 245 objects. It comprises 1262 seen compositions and 300/400 (validation/test) unseen compositions. C-GQA is a natural image dataset which contains 39298 images, with 413 attributes and 764 objects. It includes 5,592 seen compositions and 1,040/923 (validation/test) unseen compositions. VAW-CZSL is a larger dataset which contains 440 attributes and 541 objects for 238040 images, and it is split into 11175 seen and 2322/2470 unseen compositions for training and validation/testing, respectively.

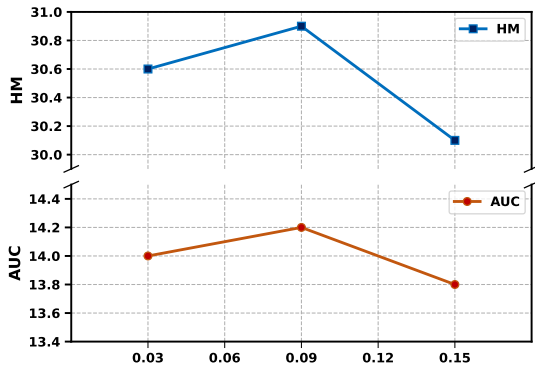


(a) MIT-States

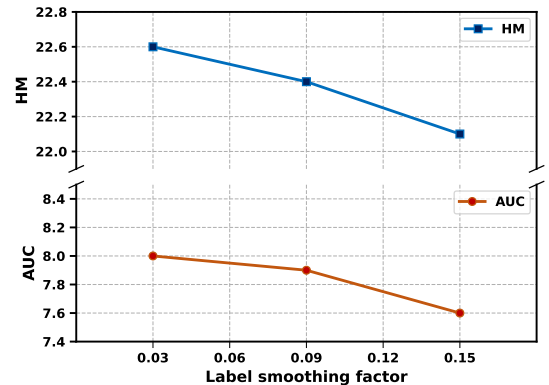


(b) C-GQA

Figure 4. Impact of the number of the visual features on (a) MIT-States and (b) C-GQA.



(a) MIT-States



(b) C-GQA

Figure 5. Impact of the label smoothing factor on (a) MIT-States and (b) C-GQA.

## D. Implementation details

We use NVIDIA PTX 3090 GPU to train all models under the Pytorch framework [31]. Since  $\mathcal{L}_{comp}$  leverages image features during training, we use a Batch Normalization, ReLU and 0.3 dropout for Image embedder. We train **TRIDENT** by Adam optimizer with weight decay  $5e-5$ , learning rates  $1.5e-6$  for word embedding as well as  $2e-4$  for other modules on three datasets. We decay the learning rate by 10 at epoch 30 and 40. The temperature variable of cosine similarity  $\delta$  is set to 0.05. For weighting coefficients  $\gamma_{ortho}$ ,  $\gamma_{comp}$ ,  $\gamma_{attr}$ , and  $\gamma_{obj}$ , we set them to 0.1, 1, 0.5, and 0.5, respectively.

## E. Impact of Hyperparameters

To provide more insight into the effect of visual features and label smoothing, we study on the performance of TRIDENT

with respect to different numbers of visual features and different label smoothing factors, respectively. Experiments exploring the impact of hyperparameters are conducted on datasets MIT-States and C-GQA.

**Impact of the number of visual features.** We illustrate the performance of TRIDENT influenced by different numbers of attribute features in Figure . In Figure 4a, the performance of our model on MIT-States generally improves with the increasing number of visual features, but subsequently declines. This trend is reasonable, as a greater number of Visual features contains more useful information, thereby enhancing the performance. However, the number of useful features is limited; thus, an excessive number of visual features may introduce redundancy and noise, ultimately hampering the performance of the model.

However, in Figure 4b, as the number of visual features increases, the performance of the model on C-GQA tends to

decline overall. This may be attributed to the model’s strong expressive capability in handling composition reasoning. In the low-noise C-GQA dataset, optimal performance can be achieved using only two features. Increasing the number of features, however, results in heightened model complexity without tangible benefits, potentially impairing generalization to unseen compositions. In contrast, the MIT-States dataset exhibits significant noise; thus, while the increase of visual features may introduce more noise, it also necessitates a greater amount of useful information, which can effectively mitigate the impact of the noise.

**Impact of the number of label smoothing factor.** The label smoothing factor  $\alpha$  modulates the extent to which the model’s confidence in seen compositions is attenuated. Figure 5a shows that as  $\alpha$  increases, the model’s performance on MIT-States initially improves before subsequently declining. This is because if alpha is too small, label smoothing fails to enhance generalization, while if alpha is too large, it adversely affects the model’s ability to learn the representation of the original labels, resulting in more losses than gains. However, as shown in Figure 5b, the model achieves the best performance with C-GQA a smaller  $\alpha$ . This may be attributed to the fact that, compared to everyday objects, LLMs are less familiar with in-the-wild objects, leading to relatively lower quality in the generated auxiliary attributes; thus, a smaller smoothing factor can mitigate the impact.